

# Low temperature growth of high-k Hf-La oxides by remote-plasma atomic layer deposition: Morphology, stoichiometry, and dielectric properties

Cite as: J. Vac. Sci. Technol. A **30**, 01A147 (2012); <https://doi.org/10.1116/1.3665419>

Submitted: 15 August 2011 • Accepted: 11 November 2011 • Published Online: 15 December 2011

Fu Tang, Chiyu Zhu, David J. Smith, et al.



View Online



Export Citation

## ARTICLES YOU MAY BE INTERESTED IN

[Film properties of low temperature HfO<sub>2</sub> grown with H<sub>2</sub>O, O<sub>3</sub>, or remote O<sub>2</sub>-plasma](#)

Journal of Vacuum Science & Technology A **32**, 01A117 (2014); <https://doi.org/10.1116/1.4842675>

[Ferroelectricity in hafnium oxide thin films](#)

Applied Physics Letters **99**, 102903 (2011); <https://doi.org/10.1063/1.3634052>

[Plasma-Assisted Atomic Layer Deposition: Basics, Opportunities, and Challenges](#)

Journal of Vacuum Science & Technology A **29**, 050801 (2011); <https://doi.org/10.1116/1.3609974>



Advance your science and  
career as a member of

AVS

LEARN MORE



# Low temperature growth of high-k Hf–La oxides by remote-plasma atomic layer deposition: Morphology, stoichiometry, and dielectric properties

Fu Tang, Chiyu Zhu, David J. Smith, and Robert J. Nemanich<sup>a)</sup>

Department of Physics, Arizona State University, Tempe, Arizona 85287-1504

(Received 15 August 2011; accepted 11 November 2011; published 15 December 2011)

In this work, we investigated the growth of Hf oxide, La oxide, and alloyed Hf–La oxide films using remote-plasma atomic layer deposition at temperatures ranging from  $\sim 80$  to  $\sim 250^\circ\text{C}$ . The relative composition and atomic bonding structure of the film were determined by *in situ* x ray photoelectron spectroscopy (XPS). Atomic force microscopy and transmission electron microscopy were implemented to characterize the morphology and crystalline structure. The XPS results indicated that for low temperature Hf oxide growth, a significant amount of excess oxygen species was observed in the deposited film. This oxygen could lead to instabilities and adversely affect the function of thin film transistors. The authors established that a He plasma post deposition treatment can partially remove the excess oxygen. In addition, the pure Hf oxide films show a surface morphology with protruding islands over a smooth surface which reflects the crystallized nature of the Hf oxide domains. In order to suppress the crystallization of the Hf oxide and to obtain a smooth morphology, 1–3 cycles of La-oxide were employed between adjacent Hf-oxide cycles. The Hf–La oxide films showed reduced roughness compared with that of the pure Hf oxide film. Carbon residue in the alloyed film is also reduced compared with that of the La oxide film. Finally, the electrical properties of the deposited films were characterized by capacitance-voltage (C-V) and current-voltage (I-V) measurement. The I-V curves show that the alloyed Hf–La oxide films have a higher break down field than that of pure Hf oxide films. © 2012 American Vacuum Society. [DOI: 10.1116/1.3665419]

## I. INTRODUCTION

High-k oxides have been widely employed in Si-based nanoscale transistors in order to reduce the gate tunneling current and energy consumption.<sup>1,2</sup> Recently, the application of high-k dielectrics is also emerging in other semiconductor areas including thin film transistors (TFTs) for flexible electronics. A high-k gate dielectric layer can significantly reduce the threshold voltage, increase the on/off current ratio and enhance the mobility of TFTs.<sup>3</sup> One of the limiting factors in implementing high-k materials for flexible electronics is the development of a low temperature deposition process.

Plasma-enhanced atomic layer deposition<sup>4–7</sup> (PEALD) has been considered as a promising approach for deposition of high-k dielectrics at low temperatures. Atomic layer deposition (ALD) is a self-limiting growth method, where growth is achieved by alternatively pulsing precursors into the deposition chamber.<sup>8,9</sup> The advantages of ALD include conformal coating, thickness uniformity, and composition and stoichiometry control. In PEALD, the excess activated oxygen species generated by the plasma can significantly reduce the deposition temperature and produce a denser film and potentially a lower defect concentration. In order to minimize the effects of the defects and excess species, studies up to now have focused on films deposited at high temperature or treated with high temperature annealing.<sup>4,6,7</sup> Neither process is appropriate for flexible substrates.

In this study, we have systematically investigated the properties of as-deposited Hf oxide, La oxide, and Hf–LaO<sub>x</sub> films using remote plasma atomic layer deposition (RPALD) at temperatures ranging from  $\sim 80$  to  $\sim 250^\circ\text{C}$ . Ion induced effects can be neglected because of the low ion density of the remote plasma treatment. The film bonding and composition were characterized with *in situ* x-ray photoemission spectroscopy (XPS); the morphology was characterized with atomic force microscopy; the crystalline structure was determined from cross section transmission electron microscopy (TEM); and the electrical properties were deduced from capacitance-voltage (C-V) and current-voltage (I-V) measurements. We found that a significant amount of excess oxygen species is observed for the Hf oxide film at low deposition temperature, which can be partially removed by a post He plasma treatment. In addition, by alloying with La, the morphology and electrical properties of the oxide film were improved.

## II. EXPERIMENT

The substrates used in this study are ambient oxidized n-type Si (100) wafers. Prior to loading the substrates into the vacuum chamber, the wafers were ultrasonically cleaned in acetone and methanol for  $\sim 15$  min duration for each process. The deposited samples were transferred to an XPS chamber through an ultrahigh vacuum (UHV) transfer line which enables *in situ* measurement without introducing contamination. The high-k oxide films were deposited using a custom computer controlled RPALD system. The base pressure of the chamber was  $\sim 1.0 \times 10^{-8}$  Torr from the turbo-drag pump

<sup>a)</sup>American Vacuum Society member. Electronic mail: robert.nemanich@asu.edu

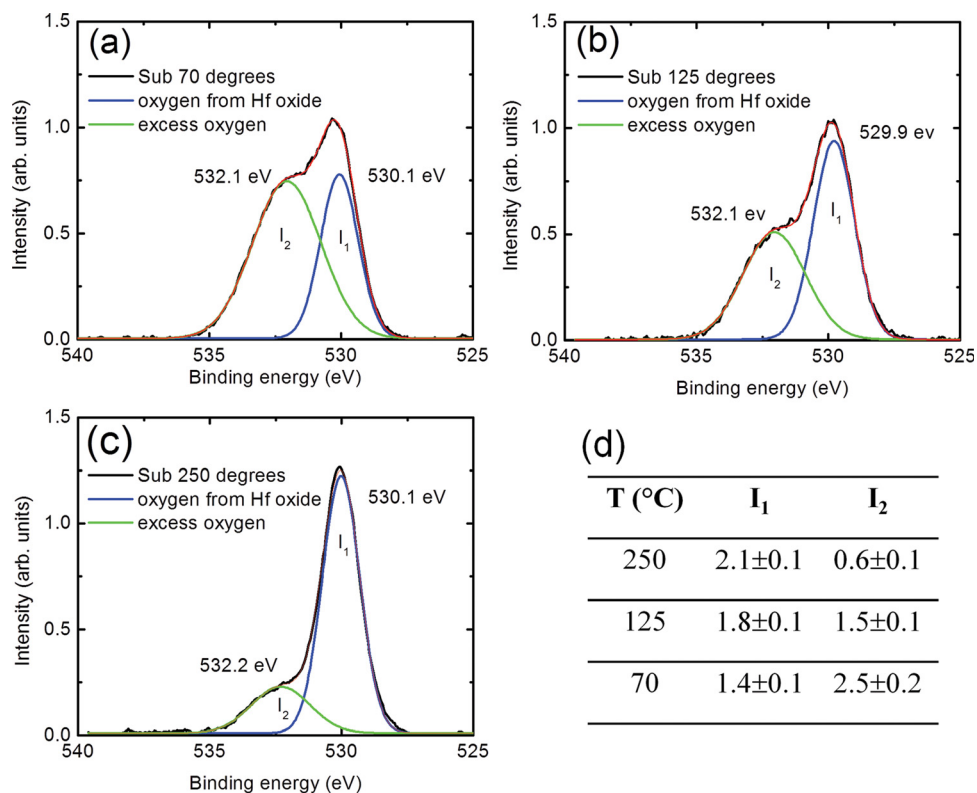


FIG. 1. (Color online) XPS O 1s spectra for Hf oxide deposited at substrate temperatures of (a) 70 °C, (b) 125 °C, and (c) 250 °C. The normalized O peak area (d) from Hf oxide ( $I_1$ ) and excess oxygen ( $I_2$ ) at different temperatures.

backed with a dry diaphragm pump. After the 0.1 s precursor pulse, the pressure increases to  $\sim 800$ – $900$  mTorr. Nitrogen gas was introduced for 10 s to purge any excess precursor. After the nitrogen purge, oxygen was introduced into the chamber for 6 s, and then excited by rf-power for 2–20 s. The pressure in the chamber during deposition was controlled by a throttle valve to a value of  $\sim 110$  mTorr. The stainless steel bubbler containing the Hf precursor (Tetrakis(ethylmethylamino)hafnium(IV)) was maintained at  $\sim 70$  °C during deposition. For the lanthanum oxide growth, the precursor Tris(isopropylcyclopenta-dienyl)lanthanum was heated to a temperature of  $\sim 168$  °C. The chamber and gas lines were heated to  $\sim 100$  °C to avoid precursor condensation. The remote plasma was excited with 13.56 MHz rf-power applied to a helical copper coil wound around a 32 mm diameter quartz tube that opens toward the sample. In these experiments the plasma power was varied from 80 to 200 W. The post-deposition He plasma treatment was excited with 35 W for a typical duration of  $\sim 20$  min. Because of the remote plasma excitation without sample bias, the sample is exposed to free radicals and excited molecules and a very low density of ions.

After deposition, the pressure was reduced in the deposition chamber, and the sample was transferred to the XPS system through the UHV linear transfer chamber. XPS characterization is performed at a base pressure of  $6 \times 10^{-10}$  Torr using the 1253.6 eV Mg K $\alpha$  line of a VG XR3 source and a VG microtech Clam II analyzer operated at a resolution of 0.1 eV. The films for XPS analysis were  $\sim 3$ – $5$  nm thick, and our prior

studies have established that charging effects can be neglected because of tunneling to the conducting Si substrates.

An Agilent 5500 AFM was used to characterize the morphology of the deposited films under tapping mode with silicon tip. Representative samples were observed in cross-section geometry using a JEOL JEM 4000EX high-resolution electron microscope operated at 400 kV. The electrical properties of the oxide films were investigated by capacitance voltage (C-V) and current voltage (I-V) measurements using a mercury probe station system (MSI Electronics Mercury Probe Hg412-3).

### III. RESULTS AND DISCUSSION

#### A. Hafnium oxide films

##### 1. Oxygen species

Figure 1 shows the XPS scan of the Hf oxide films grown on Si substrates at different temperatures. From the curves, we find that the O 1s features can be fit with two peaks. The peak at  $\sim 530$  eV is attributed to oxygen in the Hf oxide. The other peak has a higher binding energy at  $\sim 532$  eV, which has been attributed to the presence of excess oxygen species.<sup>10,11</sup> These species may include molecular oxygen or bound hydroxyl groups. At lower deposition temperatures the peak from the excess species dominates the spectrum, while at higher temperatures, this peak is significantly reduced.

Figure 1(d) presents a quantitative analysis of the oxygen 1s peak area from Hf oxide ( $I_1$ ) and the excess oxygen ( $I_2$ ).

Here,  $I_1$  or  $I_2$  are obtained from the integrated peak area divided by the atomic sensitivity factor, and each peak area has been normalized to the integrated area of the Hf 4f peaks. As the deposition temperature increases,  $I_1$  increases, suggesting increased stoichiometric bonding of the Hf and oxygen. Conversely,  $I_2$  from absorbed oxygen is reduced as the temperature is increased. The results suggest that the precursor may be not fully oxidized at low growth temperature. In addition, excess oxygen molecules or OH are weakly bonded in the film which may limit the efficiency of the atomic oxygen in the plasma. At high growth temperature, the excess oxygen species desorb, resulting in a more completely oxidized film, and the XPS is dominated by a single, narrower peak.

## 2. Post He-plasma treatment

The presence of excess oxygen may adversely affect the stability and function of TFTs. For example, the excess oxygen has been shown to form an electron surface accumulation layer which reduces the mobility of the ZnO channel layer.<sup>12,13</sup> As already noted thermal approaches employed to reduce the excess species include increasing the growth temperature or annealing the film after growth. However, for flexible electronics applications, increased temperature methods are limited because of the substrate thermal stability. An alternative method, which has been demonstrated on zinc oxide, is to expose the film to ultraviolet (UV) light.<sup>14</sup> Here, we have employed a He plasma post-deposition exposure which generates UV light dominated by  $\sim 21.2$  eV photons. Figure 2 shows the Hf and oxygen XPS peaks before and after He plasma treatment. We find that the excess oxygen peak is indeed decreased as most molecular oxygen is removed by He plasma treatment. However, the narrow oxygen peak may come from the oxygen in residue bound hydroxyl groups. Accompanying the oxygen reduction, the binding energies of both the Hf and O peaks shift by  $\sim 1.4$  eV to higher values. As the thickness of this sample is estimated as  $\sim 3$  nm, the charging effect can be neglected.

Figure 3 presents a schematic of the proposed mechanism for photo-induced desorption of the excess species in the oxide films. The presence of the excess oxygen in the film leads to sites which can accept negative charges. Thus, there will be negative charge distributed through the film, which forms a dipole structure with the positive charge in the Si substrate. This charge distribution will produce an electric field across the oxide as has been described in prior work from our laboratory.<sup>15</sup> The UV photons in the He plasma can penetrate  $\sim 13$  nm into the oxide which can induce desorption through the thickness of the film which reduces the sites available for charge transfer and the electric field across the oxide. This is consistent with the binding energy shift to higher values as observed from the XPS measurements. The XPS measurements also show that the excess oxygen is only partially released. This could be due to the fact that molecular oxygen species can be released through photo-induced desorption while other species such as hydroxyl groups still remain due to stronger bonding with the oxide.

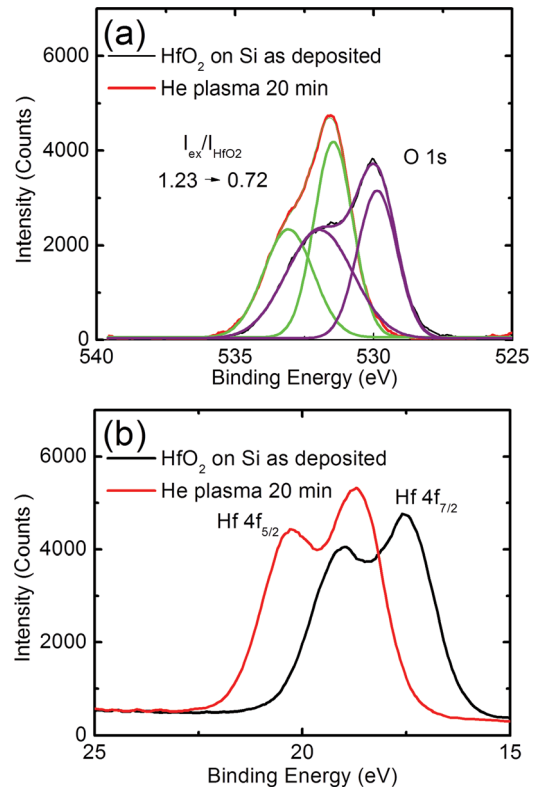


FIG. 2. (Color online) XPS spectra of (a) O 1s and (b) Hf 4f peaks, for as-deposited Hf oxide film and post He-plasma processed film.

## 3. Morphology

In addition to the excess oxygen species in the Hf oxide films, AFM measurements show that the morphology of the Hf oxide film also has some undesired features. Figure 4 presents topography images of films deposited at different plasma conditions (a) 80 W with a 8 s oxygen plasma pulse, and (b) 20 W with a 2 s oxygen plasma pulse. The morphology of both films showed similar features: a number of protruding islands extending beyond the smooth surface. The average thickness of the films is  $\sim 10$  nm; however, the peak-valley height can reach  $\sim 20$  nm. In the case of high oxygen plasma power and long plasma exposure, the density of protruding islands was slightly increased. These protruding islands are presumed to be crystallized grains, as found by Hausmann *et al.*<sup>16</sup> Even with the plasma power reduced to 20 W and a short exposure time of 2 s, significant crystallization was still detected.

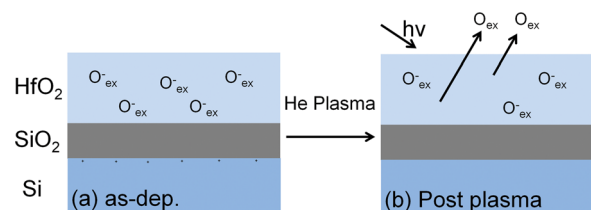


FIG. 3. (Color online) Schematic of the proposed mechanism for oxygen desorption induced by the He plasma process: (a) the excess oxygen in the as-deposited Hf oxide film and (b) oxygen desorbed from the film during ultraviolet light (UV) illumination generated from the He plasma.

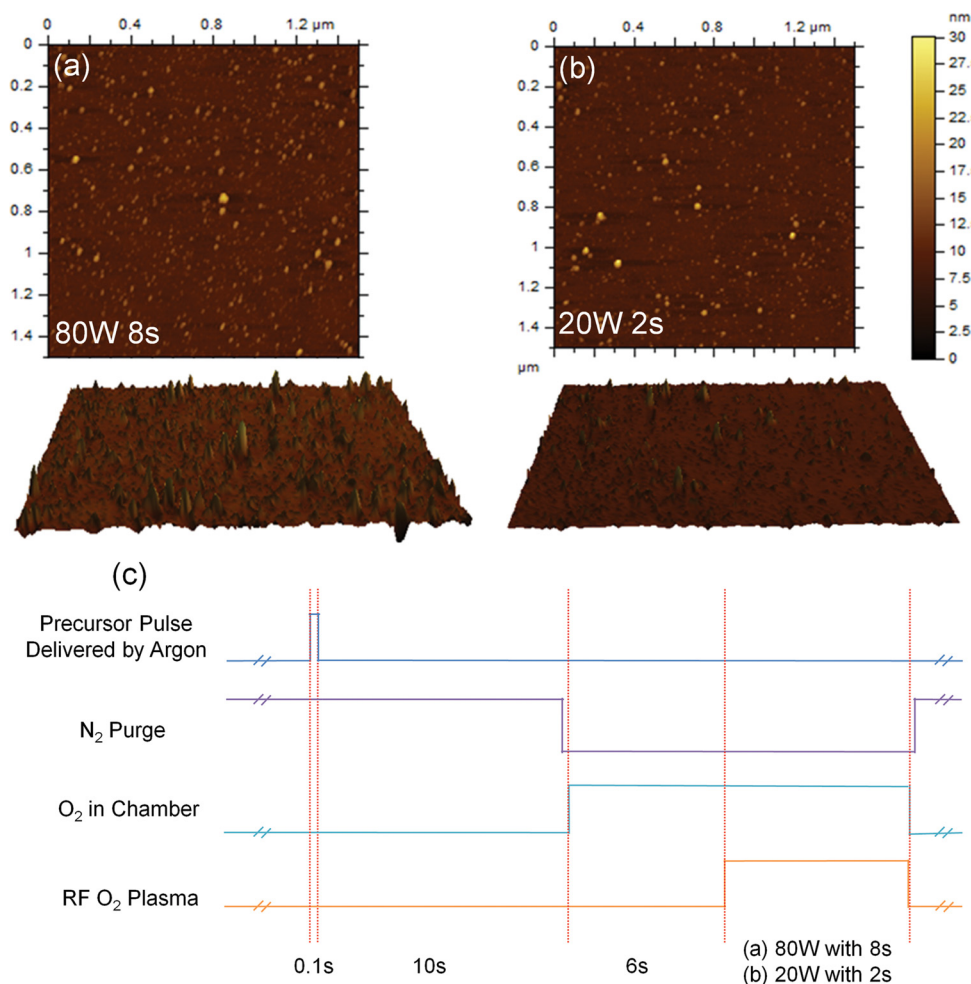


FIG. 4. (Color online) AFM topography images of Hf oxide films deposited with O plasma pulse conditions of (a) 80 W and 8 s exposure, (b) 20 W and 2 s exposure, and (c) the ALD processing sequence.

## B. La oxide films

Figure 5 presents AFM and XPS results of La oxide films deposited with different plasma power and oxygen exposure times. Both films have a smooth surface without protruding islands, consistent with the amorphous nature typically obtained for La oxides.<sup>17,18</sup> Although the morphology is improved, the XPS indicates the presence of a significant amount of carbon in the deposited films (see Fig. 5). The feature normally associated with adventitious surface carbon at  $\sim 284$  eV is hardly evident. With higher power or longer oxygen plasma exposure, the carbon concentration can be reduced. The binding energy of the C 1s peak shifts from  $\sim 291$  to  $\sim 290$  eV depending on the conditions employed for the oxygen plasma step. This range of binding energy is close to the value for carbon bonded in a carbonate structure, which indicates the oxidation of the carbon. This detection of carbon oxide could be due to the absorption of CO<sub>2</sub> and formation of La<sub>2</sub>O<sub>2</sub>CO<sub>3</sub> during the growth of La oxide.<sup>19</sup>

## C. Hf–La oxide films

In order to suppress crystallization of the Hf oxide film, we deposited alloyed Hf–La oxide films by growing 1–3

cycles of La-oxide between two adjacent Hf-oxide cycles. This approach has also been employed at higher deposition temperatures using thermal ALD.<sup>20–22</sup> The relative percentages of Hf and La in the alloyed films can be controlled by the ratio of the number of Hf and La cycles. As shown in Fig. 6, AFM images of the alloyed Hf–La oxide films display a significant reduction in the density of protruding islands compared with that of pure Hf oxide films. The thickness of the films is  $\sim 7$  nm. For the film grown with a 1La/1Hf cycle ratio, a number of tall islands are observable protruding from the surface. When the cycle ratio is increased to 2La/1Hf, the density of protruding island is suppressed. In Fig. 6(c), an analysis of the element concentration is listed. From the figure, it is evident that carbon in the alloyed films can be controlled to a relatively low value of  $\sim 1.6\%$ . This result suggests that the incorporated Hf inhibits the formation of La carbonate (La<sub>2</sub>O<sub>2</sub>CO<sub>3</sub>) during the ALD growth.

### 1. Film crystallinity

Figure 7 shows cross-sectional electron micrographs of the pure Hf oxide film and the alloyed Hf–La oxide film. It

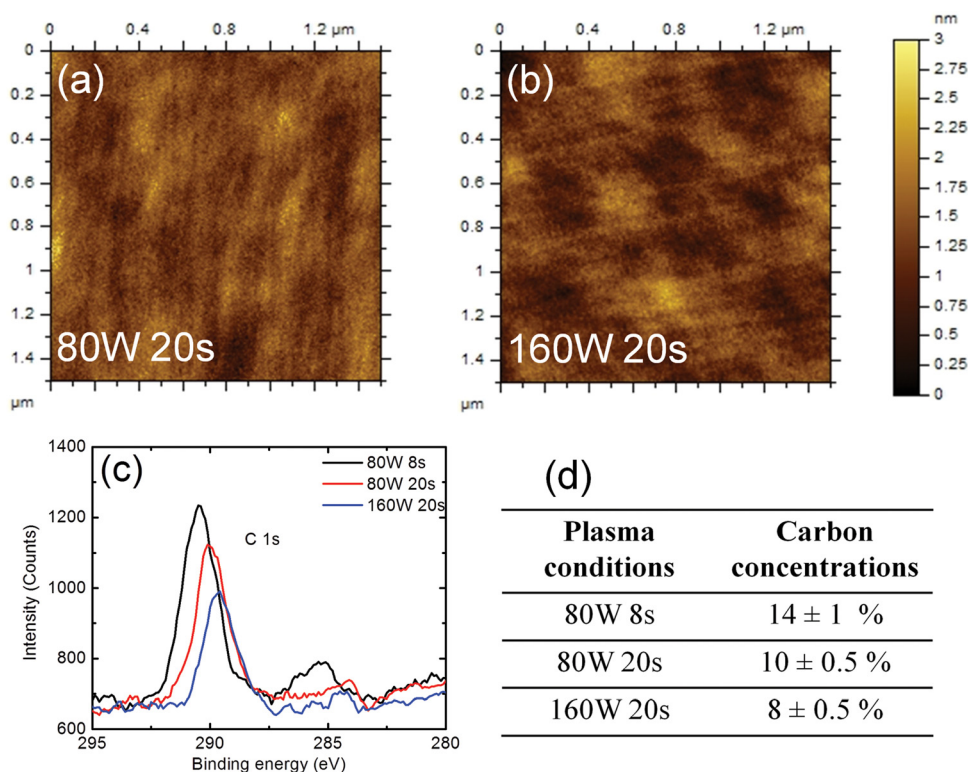


FIG. 5. (Color online) AFM topography images of La oxide films deposited with O plasma pulse conditions of (a) 80 W and 20 s exposure and (b) 160 W and 20 s exposure; (c) XPS spectra of the C 1s peak and (d) carbon concentrations of La oxide films deposited with different O plasma pulse conditions.

is evident that micro-crystalline domains extend through the entire thickness of the Hf oxide. The existence of such grain boundaries is often associated with enhanced leakage current. For the alloyed film, electron micrographs did not

reveal evidence for distinct crystalline structures; thus indicating an amorphous structure for the alloy. These observations are consistent with the conclusions deduced from the AFM measurements.

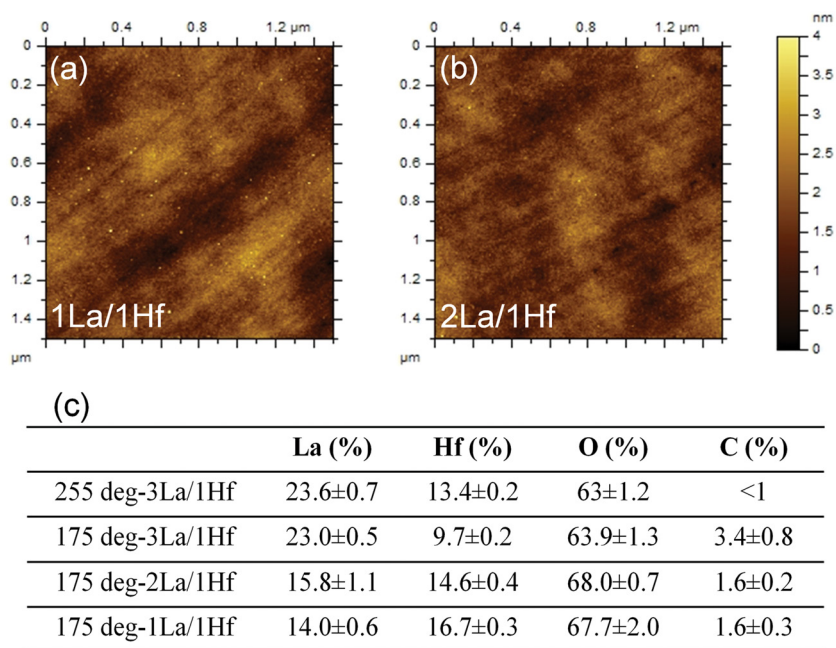


FIG. 6. (Color online) AFM topography images of the oxide film deposited with different cycle ratios: (a) 1La/1Hf and (b) 2La/1Hf; (c) atomic concentrations.

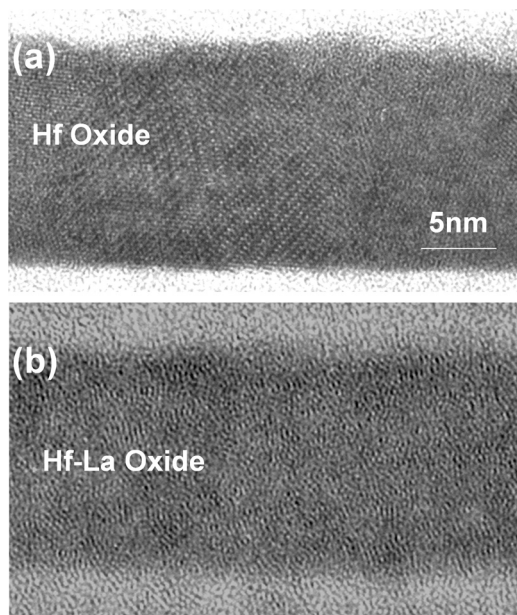


FIG. 7. Cross sectional TEM images of (a) pure Hf oxide and (b) alloyed oxide film with a 2La/1Hf cycle ratio.

## 2. Electrical properties

A mercury probe was employed to measure the capacitance versus voltage at low frequency for the deposited oxide film. Using the low frequency results, we found that the effective dielectric constants of the pure Hf oxide film and alloyed Hf-La oxide films were  $18.1 \pm 1.2$  and  $14.2 \pm 1.5$ , respectively. Figures 8(a) and 8(b) show I-V curves of pure Hf oxide and alloyed Hf-La oxide just before breakdown.

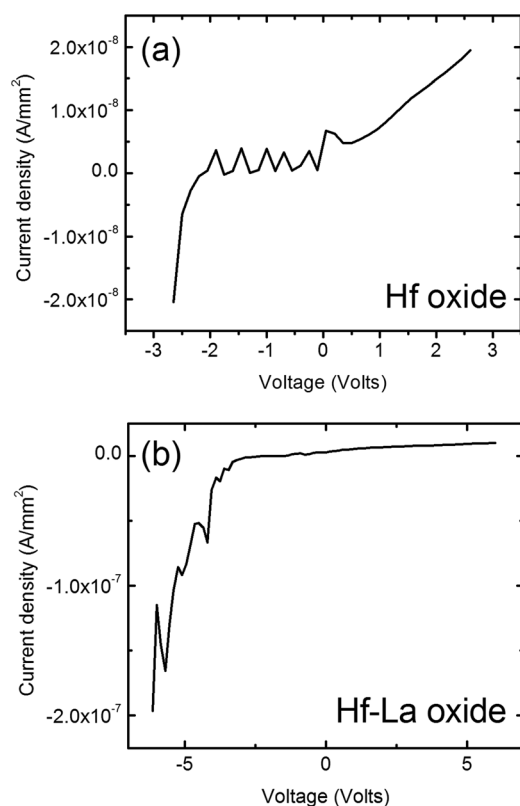


FIG. 8. I-V curves of (a) pure Hf oxide and (b) alloyed oxide film.

We found that the alloyed Hf-La oxide film has a breakdown strength of  $3.0 \pm 0.3$  MV/cm while the breakdown strength of the pure Hf oxide film is  $1.4 \pm 0.2$  MV/cm. He *et al.*<sup>20</sup> also reported a higher breakdown field for alloyed Hf-La oxide than that of pure Hf oxide after the films were annealed to above 500 °C.

## IV. CONCLUSIONS

We have found (1) significant excess oxygen species are present in Hf oxide films deposited at low temperature by RPALD, which can be partially removed by a post He plasma treatment; (2) crystallized grains protrude from the surface of Hf oxide films even when using low rf power to excite the oxygen plasma and a short exposure time; (3) the alloyed Hf-La oxide film displays a smooth surface and low C concentration; and (4) the alloyed Hf-La oxide film has a higher breakdown voltage than that of a pure Hf oxide film consistent with an amorphous structure.

## ACKNOWLEDGMENTS

This work was supported through US Army Cooperative Agreement No. W911NF-04-2-0005 (FDC-10-4.6). Doug Loy and Barry O'Brien are acknowledged for helpful discussions.

- <sup>1</sup>A. I. Kingon, J. P. Maria, and S. K. Streiffer, *Nature* **406**, 1032 (2000).
- <sup>2</sup>G. D. Wilk, R. M. Wallace, and J. M. Anthony, *J. Appl. Phys.* **89**, 5243 (2001).
- <sup>3</sup>B. H. Lee, K. H. Lee, S. Im, and M. M. Sung, *Org. Electron.* **9**, 1146 (2008).
- <sup>4</sup>P. K. Park, J. S. Roh, B. H. Choi, and S. W. Kang, *Electrochem. Solid State Lett.* **9**, F34 (2006).
- <sup>5</sup>J. S. Park, H. S. Park, and S. W. Kang, *J. Electrochem. Soc.* **149**, C28 (2002).
- <sup>6</sup>Y. Won, S. Park, J. Koo, S. Kim, J. Kim, and H. Jeon, *Appl. Phys. Lett.* **87**, 262901 (2005).
- <sup>7</sup>S. Choi, J. Koo, H. Jeon, and Y. Kim, *J. Korean Phys. Soc.* **44**, 35 (2004).
- <sup>8</sup>M. Leskela and M. Ritala, *Thin Solid Films* **409**, 138 (2002).
- <sup>9</sup>T. Suntola, *Thin Solid Films* **216**, 84 (1992).
- <sup>10</sup>L. Belau, J. Y. Park, T. Liang, and G. A. Somorjai, *J. Vac. Sci. Technol. B* **26**, 2225 (2008).
- <sup>11</sup>C. Driemeier, R. M. Wallace, and I. J. R. Baumvol, *J. Appl. Phys.* **102**, 024112 (2007).
- <sup>12</sup>S. Lee, S. Bang, J. Park, S. Park, W. Jeong, and H. Jeon, *Phys. Status Solidi A* **207**, 1845 (2010).
- <sup>13</sup>S. Song, W. K. Hong, S. S. Kwon, and T. Lee, *Appl. Phys. Lett.* **92**, 263109 (2008).
- <sup>14</sup>H. Kind, H. Q. Yan, B. Messer, M. Law, and P. D. Yang, *Adv. Mater.* **14**, 158 (2002).
- <sup>15</sup>C. C. Fulton, G. Lucovsky, and R. J. Nemanich, *J. Appl. Phys.* **99**, 063708 (2006).
- <sup>16</sup>D. M. Hausmann and R. G. Gordon, *J. Cryst. Growth* **249**, 251 (2003).
- <sup>17</sup>Jin-Bo Chengb, Ai-Dong Li, Qi-Yue Shao, Hui-Qin Ling, Di Wu, Yuan Wang, Yong-Jun Bao, Mu Wang, Zhi-Guo Liu, and Nai-Ben Ming, *Appl. Surf. Sci.* **233**, 91 (2004).
- <sup>18</sup>K. Kukli, M. Ritala, V. Pore, M. Leskelä, T. Sajavaara, R. I. Hegde, D. C. Gilmer, P. J. Tobin, A. C. Jones, and H. C. Aspinall, *Chem. Vap. Deposition*, **12**, 158 (2006).
- <sup>19</sup>M. Nieminen, M. Putkonen, and L. Niinisto, *Appl. Surf. Sci.* **174**, 155 (2001).
- <sup>20</sup>W. He, D. S. H. Chan, S. J. Kim, Y. S. Kim, S. T. Kim, and B. J. Cho, *J. Electrochem. Soc.* **155**, G189 (2008).
- <sup>21</sup>T. Wang and J. G. Ekerdt, *Chem. Mater.* **21**, 3096 (2009).
- <sup>22</sup>T. Wang and J. G. Ekerdt, *Chem. Mater.* **22**, 3798 (2010).